AGU PUBLICATIONS

Geophysical Research Letters

RESEARCH LETTER
10.1002/2016GL070262

Key Points:
- The relocation of SAL dust by a tropical storm has been quantified in a numerical simulation
- A unique dust mass tracking and budgeting method has been employed in this study
- The dust mass removed to the surface was found to be ~75 times more than that transported aloft

Correspondence to:
S. R. Herbener,
stephen.herbener@colostate.edu

Citation:
Herbener, S. R., S. M. Saleeby, S. C. van den Heever, and C. H. Twohy (2016), Tropical storm redistribution of Saharan dust to the upper troposphere and ocean surface, *Geophys. Res. Lett.*, *43*, 10,463–10,471, doi:10.1002/2016GL070262.

Received 2 JUL 2016
Accepted 20 SEP 2016
Accepted article online 22 SEP 2016
Published online 9 OCT 2016

Tropical storm redistribution of Saharan dust to the upper troposphere and ocean surface

Stephen R. Herbener[1], Stephen M. Saleeby[1], Susan C. van den Heever[1], and Cynthia H. Twohy[2]

[1]Department of Atmospheric Science, Colorado State University, Fort Collins, Colorado, USA, [2]NorthWest Research Associates, Redmond, Washington, USA

Abstract As a tropical cyclone traverses the Saharan Air Layer (SAL), the storm will spatially redistribute the dust from the SAL. Dust deposited on the surface may affect ocean fertilization, and dust transported to the upper levels of the troposphere may impact radiative forcing. This study explores the relative amounts of dust that are vertically redistributed when a tropical cyclone crosses the SAL. The Regional Atmospheric Modeling System (RAMS) was configured to simulate the passage of Tropical Storm Debby (2006) through the SAL. A dust mass budget approach has been applied, enabled by a novel dust mass tracking capability of the model, to determine the amounts of dust deposited on the ocean surface and transferred aloft. The mass of dust removed to the ocean surface was predicted to be nearly 2 orders of magnitude greater than the amount of dust transported to the upper troposphere.

1. Introduction

The vertical location of aerosol particles significantly influences the Earth's radiation budget [*Maring et al.*, 2003; *Zarzycki and Bond*, 2010; *Reddy et al.*, 2013]. Dust also serves effectively as both cloud condensation nuclei (CCN) and ice nucleating particles (INP) [*DeMott et al.*, 2003], and thus, the interaction of dust with storms can have a significant impact on the microphysical processes and the associated cloud radiative forcing [e.g., *Twomey*, 1974; *Albrecht*, 1989; *Heymsfield and McFarquhar*, 2001; *Seigel et al.*, 2013]. The redistribution of mineral dust also affects the Earth's biosystem. Dust deposited on the ocean surface may lead to the fertilization of ocean animal and plant life [e.g., *Babin et al.*, 2004]. Therefore, the amount and location of dust within the atmosphere has important implications for the overall Earth system.

As precipitation intensity, updraft strengths, and the altitudes of storm detrainment vary substantially as a function of storm type [*Cotton et al.*, 1995], different convective storm types could be expected to have very different impacts on the vertical redistribution of dust. Furthermore, dust ingestion pathways into deep convection are not always evident, and the amount of dust processed by a storm can vary greatly with environmental conditions [*Seigel and van den Heever*, 2012]. All of these concepts underscore the need to understand the cloud processes that influence the transport and redistribution of dust.

Aerosols may be redistributed via a number of pathways including removal from the atmosphere by precipitation and convective transport to upper levels. For example, *Mishra and Shibata* [2012] found that deep convection carries aerosol particles to upper levels during the premonsoon season over the central Indo-Gangetic Belt, and that during the monsoon season, precipitation removes a significant number of particulates from the atmosphere.

The study mentioned above is based upon observational data. In this study, we utilize a cloud-resolving model (CRM) to examine how convective transport and precipitation associated with a tropical cyclone (TC) impact the vertical profile of dust in the Saharan Air Layer (SAL). The goal of this study is to quantitatively determine how much dust is removed to the surface and is transported to the upper troposphere when a TC passes through the SAL. Addressing these goals will enhance our understanding of the role of TCs in global dust transport, and how the SAL is modified by TCs.

2. Model Description and Configuration

Regional Atmospheric Modeling System (RAMS), a nonhydrostatic CRM that features a two-moment bin-emulating bulk microphysical scheme [*Walko et al.*, 1995; *Meyers et al.*, 1997; *Cotton et al.*, 2003; *Saleeby and Cotton*, 2004], was utilized for this study. Cloud, rain, pristine ice, snow, aggregate, graupel, and hail

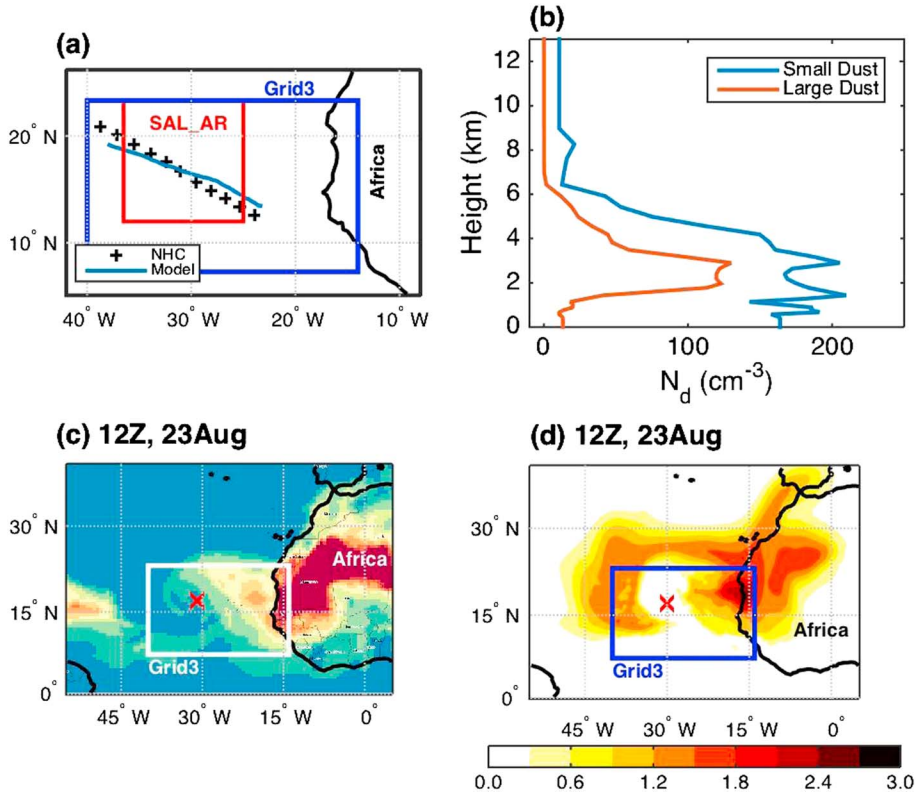

Figure 1. (a) TS Debby (2006) storm track, comparing the National Hurricane Center Best Track observations ("+" symbols) with the simulated storm (blue). Storm track data begin at 06 Z, 22 August 2006 (southeast endpoint) and end at 18 Z, 24 August 2006 (northwest endpoint). The horizontal extent of the SAL Analysis Region (SAL_AR, see text) is marked in red. (b) Initial dust number concentration (cm^{-3}) profiles based on NAMMA observations. (c) MERRA-2 dust column mass density ($g\,m^{-2}$) for 12 Z, 23 August 2006 (contour colors range linearly from 0, blue, to 1 $g\,m^{-2}$, brown) and (d) vertically integrated dust mass (M_D, $g\,m^{-2}$) from the simulated time 12 Z, 23 August 2006. The horizontal extent of model grid3 is shown (blue or white) in Figures 1a, 1c, and 1d, and the horizontal extent of model grid1 is beyond the boundaries of the maps displayed in Figures 1a, 1c, and 1d. Storm center is marked by red "X" in Figures 1c and 1d.

hydrometeor species were enabled in order to capture the mixed-phase cloud processes associated with deep tropical convection. Droplet nucleation can occur at any level where available CCN and appropriate water supersaturation coexist. Homogeneous freezing begins to initiate weakly at −30°C and the rate of freezing increases at colder temperatures [*DeMott et al*., 1994]. In mixed-phase regions, cloud water can be transferred to ice species by riming, the Bergeron-Findeisen process, and homogeneous freezing. An improved heterogeneous ice nucleation scheme based on the parameterization by *DeMott et al*. [2015] was applied [*Saleeby and van den Heever*, 2013]. Three distinct aerosol species were used: sulfate, mineral dust, and sea salt. The separate aerosol species do not interact, however, the regenerated aerosol category may be comprised of a mixture of the various species. Aerosols were configured to be radiatively active in the simulations [*Harrington*, 1997; *Stokowski*, 2005] since mineral dust can absorb and scatter solar radiation.

The model domain consisted of two-way, triple-nested Arakawa-C grids [*Mesinger and Arakawa*, 1976]. The outer domain extent (12,000 km by 6000 km) was sufficiently large to capture the African Easterly Wave that generated Tropical Storm (TS) Debby, and the inner domain extent (2800 km by 1800 km) contained Debby's track over a period of sixty hours (Figure 1a). Horizontal spacing was set to 30 km, 15 km, and 3 km, respectively, for the outermost to innermost grids, respectively. Fifty-six vertical levels were defined with stretched spacing ranging from 50 m near the surface to 1000 m in the upper troposphere. The two outer domains utilized a modified Kuo cumulus parameterization [*Molinari*, 1985], while the inner domain had full microphysics [*Saleeby and van den Heever*, 2013] enabled. Dust present in the outer grids (with cumulus parameterization) can still be redistributed via convective transport since the parameterization will influence vertical motion and the dust is subject to advection. The simulation was run from 12 Z, 20 August 2006 to 18 Z, 24 August 2006.

The analysis period consisted of the final 60 h of the simulation (06 Z, 22 August to 18 Z, 24 August). The start of the analysis period (06 Z, 22 August) coincided with when Debby had developed into a tropical depression but before Debby had entered the SAL.

The model initialization and configuration were designed to recreate conditions similar to those present when TS Debby passed through the SAL. This event was observed during the NASA African Monsoon Multidisciplinary Analysis (NAMMA) campaign [*Zipser et al.*, 2009]. Global Data Assimilation System-Final reanalysis data were employed to initialize the RAMS simulation, including the warm dry air layer associated with the SAL, and for the lateral boundary conditions. Dust vertical profiles (Figure 1b), based on aircraft aerosol measurements from NAMMA [*Chen et al.*, 2011], were applied horizontally homogeneously within the confines of the SAL at the beginning of the analysis period (06 Z, 22 August). The model utilized "small" and "large" dust modes based on NAMMA observations [*Chen et al.*, 2011] with median diameters (D_m) of 0.1 and 1.0 μm, respectively. The dust was assumed to be mildly hygroscopic [*Twohy et al.*, 2009] and therefore could act as both CCN and INP.

In the model TS Debby began to encounter the SAL at approximately 0 Z, 23 August (18 h into the simulation), thus giving the model sufficient time to distribute the dust three dimensionally from the initial horizontally homogeneous field. All grids were initialized with dust in the identified SAL region, and dust was advected across the nested grid boundaries. Some recent modeling studies have initialized their dust fields with satellite data sets constrained by MODIS [e.g., *Reale et al.*, 2014] so that the effects of dust upon the storm could be assessed using fields that closely approximate those of MODIS. The current study, however, investigates the impact of the storm on the dust field with a focus on how the vertical distribution of the dust field is altered. For this reason, we initialize the dust field using vertical profiles based on in situ measurements, and let it be freely redistributed and acted upon by the motions resolved on the cloud and mesoscale and the associated microphysical processes.

Sulfate and sea-salt particles were also included in this study in order to recreate general marine aerosol conditions unrelated to the SAL [*Heymsfield and McFarquhar*, 2001; *Hudson and Yum*, 2002]. At the beginning of the analysis period, the sulfate aerosol mode ($D_m = 0.15$ μm) was introduced horizontally homogeneously across the entire simulation domain with a vertical profile representing typical marine clean conditions ($N = 100\ \mathrm{cm}^{-3}$ near the surface, exponentially decaying with increasing altitude). The sea-salt aerosols (three size modes: $D_m = 0.2$ μm, 2.0 μm, and 12 μm) were dynamically introduced into the model through a built-in surface emission source [*Saleeby and van den Heever*, 2013].

RAMS simulates the following three processes that can result in the removal of airborne aerosols to the surface: nucleation scavenging, collisional scavenging, and gravitational settling (dry deposition) [*Saleeby and van den Heever*, 2013]. Nucleation scavenging represents the sequence of aerosols nucleating cloud droplets or pristine ice that subsequently may form precipitation that falls, thereby transporting the aerosol mass to the surface. Collisional scavenging is the collection of aerosol particles by hydrometeors as they fall and hence can subsequently transport the captured aerosol mass to the surface in precipitation. Wet deposition is the sum of aerosol mass transferred to the surface through both of these processes.

3. Methodology

The analysis presented here was conducted within a region, denoted "SAL Analysis Region" (SAL_AR), which covers a large portion of the SAL within grid3 (Figure 1a). The SAL_AR was used to quantitatively analyze the impact that TS Debby had on the vertical distribution of SAL dust. In order to accomplish this, an innovative dust tracking and budget approach was utilized, as described below. Because the absolute amount of dust transported is dependent upon the size of the SAL_AR, all dust mass quantities were normalized by the total amount of dust mass within the SAL_AR at the time dust was introduced into the model (06 Z, 22 August).

RAMS uniquely tracks the mass of dust at every point and every time step throughout the simulation [*Saleeby and van den Heever*, 2013]. Unprocessed (interstitial, nonactivated) dust mass will be denoted "M_D" in this study. Any dust mass subjected to nucleation and collection by precipitation processes will transfer to another category that represents dust embedded within hydrometeors that is denoted "M_{DHY}". From the M_{DHY} category, dust particles can reenter the atmosphere after evaporation or sublimation. This dust mass is termed "regenerated dust" [*Saleeby and van den Heever*, 2013] and is denoted "M_{DRGN}." Dust mass can also be transferred to the surface, via wet and dry deposition. This mass is denoted "M_{DSFC}."

For budgetary purposes, M_D represents all of the dust in the analysis region at the start of the analysis period (06 Z, 22 August), and all other RAMS tracked dust mass categories (M_{DHY}, M_{DRGN}, and M_{DSFC}) were treated as sinks of M_D since particles existing in the M_{DHY}, M_{DRGN}, and M_{DSFC} types initially came from the M_D category and thus represent processes by which M_D is depleted. The SAL in the model extended beyond the SAL_AR region meaning that horizontal advection also acted as either a source or sink of dust mass with respect to the SAL_AR. Horizontal dust advection can impact all of the tracked dust mass categories except for M_{DSFC}. Advective contributions to the mass change in the M_{DHY} and M_{DRGN} categories were small, arising primarily from storm motion, and hence were not separated out from these categories. However, as this was not the case for M_D, mass changes in M_D due to horizontal dust advection were accounted for in the budget and calculated as a budget residual. This dust mass is denoted "M_{DADV}." Since dust mass is separated into the M_{DADV} and M_{DRGN} categories, this allows for the discernment between dust mass that was transported due to action outside the storm (advection) from that inside the storm (convective transport).

A budget was then constructed for the total amount of dust mass removed from M_D within the SAL_AR, which consists of the sum of M_{DHY}, M_{DRGN}, M_{DSFC}, and M_{DADV}. This dust mass budget was then utilized to address how much dust is removed to the surface and how much dust is transported to upper levels when a TC passes through the SAL, where M_{DSFC} directly answers the former question, while examining M_{DHY} and M_{DRGN} at levels above the SAL will address the latter.

As TS Debby traverses across the SAL, one would expect the amount of dust transported aloft to increase as the storm enters the SAL, attain a maximum value while the storm is inside the SAL, and then decrease as the storm exits the SAL. The extent of the SAL_AR was chosen in order to place the center of the simulated storm outside the SAL_AR both at the start and end of the analysis period (Figure 1a) with the purpose of capturing the aforementioned maximum. After the passage of the storm, most of the dust in M_{DHY} will eventually transfer to M_{DRGN} due to the sublimation and evaporation of remnant anvils, leaving M_{DRGN} the better representative of how much dust had been transported aloft. A volume integration of M_{DRGN} was performed at each time step in order to create a time series of dust mass (Figure 3d). Evaluation of the following integral on the M_{DRGN} time series yields the total regenerated dust mass lofted by the storm ($M_{DRGN,LOFT}$):

$$M_{DRGN,LOFT} = \int_{t_i}^{t_f} \frac{dM_{DRGN}}{dt} dt, \quad (1)$$

where t_i is the initial time and t_f is the final time of the evaluation interval. The limits of integration were chosen to range from 30 min after the onset of the analysis period to the point where the time series of M_{DRGN} attained its maximum value. The 30 min offset from the beginning of the analysis period was used to separate preexisting dust residing at upper levels due to model initialization from the dust that was lofted by the storm. The maximum value of the M_{DRGN} time series was selected in order to gain a meaningful result that reveals the upper limit of the amount of dust lofted by the storm.

4. Results

4.1. Simulated Dust Redistribution

The simulated interaction of TS Debby and the SAL constitutes a reasonable facsimile of observations (Figure 1). The model storm center was determined using the centroid of minimum sea level pressure [*Nguyen et al.*, 2014], and the storm track aligns well with the National Hurricane Center Best Track data (Figure 1a). The spatial distribution of vertically integrated M_D from the model (Figure 1d) bears a noticeable resemblance to MERRA-2 observations (Figure 1c) in terms of the horizontal distribution. Both storms are located roughly in the same place (observations 17 N, 31 W; model 17 N, 30 W), and both images (Figures 1c and 1d) show evidence of the storm clearing a pathway in the dust field and wrapping dust around the storm periphery in association with the storm rotation.

As TS Debby traverses through the SAL_AR, the midlevel dusty air layer associated with the SAL is modified in regard to the vertical distribution of dust (Figure 2a). The majority of dust mass is located between 2 and 3 km height at the beginning of the analysis period (Figure 2a). By the end of the analysis period (18 Z, 24 August), the vertical profile of M_D has been modified to one with more evenly distributed dust mass between 1 and 5 km altitudes (Figure 2a). As the simulation progresses, M_{DHY} and M_{DRGN} increase both below and above the freezing level (~5.5 km elevation), although the amounts above the freezing level are small compared

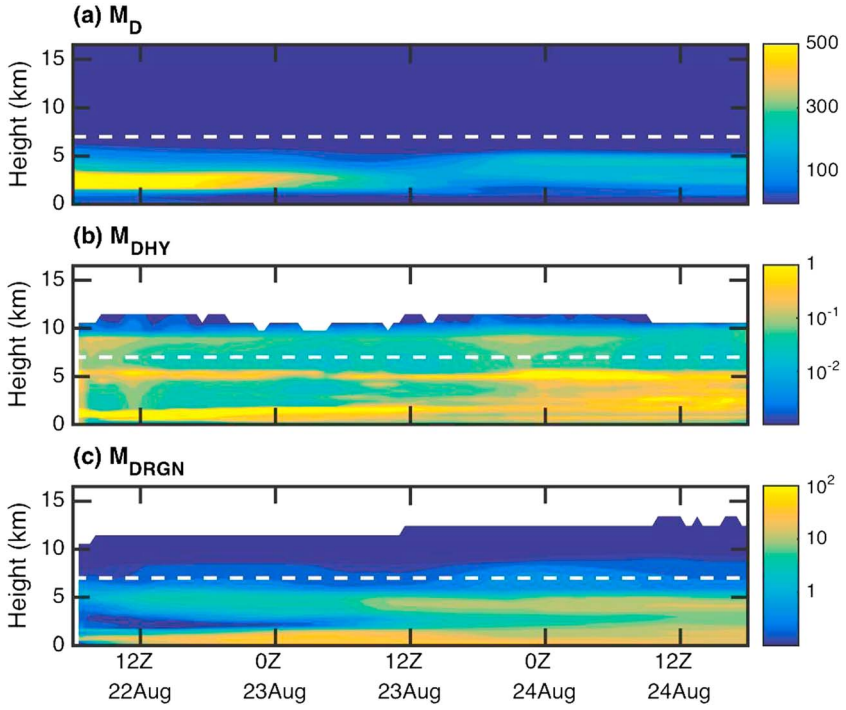

Figure 2. Hovmöller diagrams of horizontally averaged (a) unprocessed dust mass (M_D, $\mu g\,m^{-3}$), (b) dust mass within hydrometeors (M_{DHY}, $\mu g\,m^{-3}$), and (c) regenerated dust mass (M_{DRGN}, $\mu g\,m^{-3}$) within the SAL_AR. Note different color scales in Figures 2a–2c. The white dashed lines denote 7 km altitude, which is the level used to separate the SAL and upper level regions.

with those lower down (Figures 2b and 2c). The lack of M_{DHY} between 2 and 5 km heights at the start of the analysis period (Figure 2b) indicates the existence of the warm, dry midlevel air layer characteristic of the SAL preceding the entry of the storm into the SAL_AR. As the storm travels through the SAL_AR, it brings moisture along with it resulting in the appearance of M_{DHY} from the surface to 5 km altitude as seen toward the end of the analysis period (Figure 2b). The white dashed lines in Figure 2 mark the 7 km altitude, the level used to separate the SAL levels from the upper levels of the SAL_AR. This altitude was selected because it is above the SAL but below the outflow levels of the storm.

4.2. Dust Removal

Horizontal advection (M_{DADV}) has the most significant impact on the changes of M_D within the analysis region (Figures 3a and 3c). During the first half of the simulation (06 Z, 22 August to 12 Z, 23 August), M_D is removed mainly due to advection although the other budget terms also increase as the storm traverses the SAL (Figure 3c). During the second half of the simulation (12 Z, 23 August to 18 Z, 24 August), M_D is restored by advection (Figures 3a and 3c), apparently due to dust getting wrapped around the storm as suggested by Figure 1d. The other budget terms remain constant or decrease (Figure 3c) during this time period.

Although dust aerosols become embedded within both ice and liquid hydrometeors, the majority of M_{DHY} is located below the freezing level (5.5 km height) and is therefore predominantly contained within liquid hydrometeors (Figure 2b). The average precipitation rate within the SAL_AR builds during the first half of the analysis period and then tapers off (Figure 3b) resulting in the continuous accumulation of dust mass at the surface (M_{DSFC}, Figure 3c). The total accumulation of M_{DSFC} at the end of the simulation represents ~3% of the dust mass (M_D) that was introduced within the SAL_AR at the onset of the analysis period. M_{DSFC} contains dust transported to the surface via wet and dry deposition; however, the relatively slow settling time [*Saleeby and van den Heever*, 2013] in context of the 60 h analysis period implies that nearly all of M_{DSFC} arrived from wet deposition.

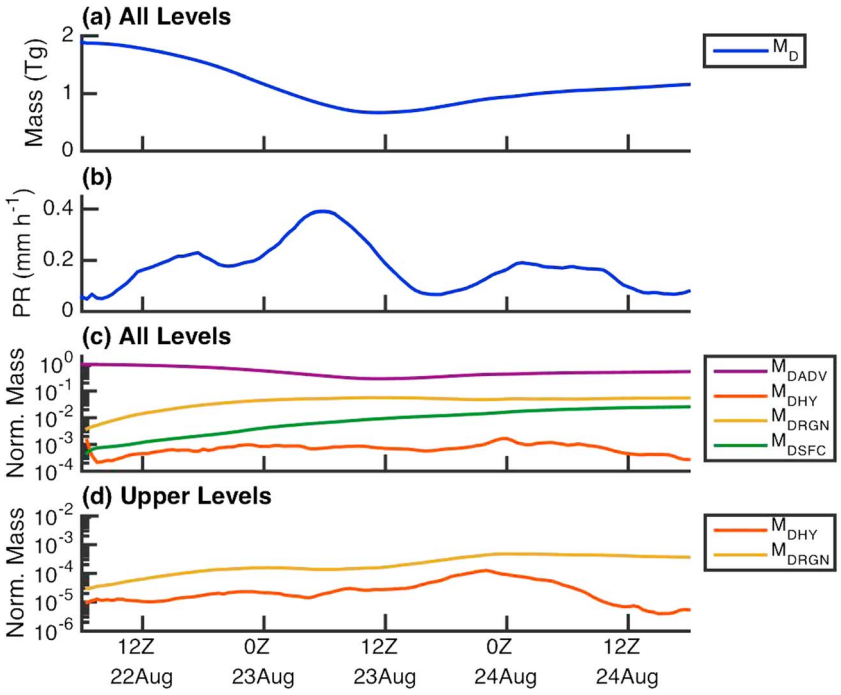

Figure 3. Time series of (a) volume integrated M_D (Tg) for all levels, (b) average precipitation rate (mm h^{-1}), and normalized volume integrated dust mass for (c) all levels and (d) upper levels within the SAL_AR. For Figures 3c and 3d, normalization is relative to the volume integrated M_D amount within the SAL_AR (for all levels) that was introduced at the beginning of the analysis period (06 Z, 22 August). "All levels" is defined as the vertical range between the surface and the tropopause (16.5 km altitude), and "upper levels" is defined as the vertical range between 7 km elevation and the tropopause. All values shown are instantaneous values except for M_{DSFC} which is an accumulated value.

4.3. Dust Transport to Upper Levels

Deep convection associated with TS Debby lifts dust from the SAL, located at low to midlevels (Figure 2a), above 7 km to the upper troposphere. M_{DHY} increases until 22 Z, 23 August after which it decreases (Figure 3d). This result is consistent with the passage of Debby through the SAL_AR. As the storm enters the SAL_AR, the amount of condensate present at upper levels within the SAL_AR increases due to the convective activity associated with the storm. As Debby travels across the SAL_AR, the amount of upper level condensate attains a maximum and eventually decreases as the storm exits the SAL_AR and/or weakens. A similar trend in M_{DHY} appears since a portion of the condensate associated with the storm contains embedded dust particles.

A progression is seen with M_{DRGN} comparable to that of M_{DHY} (Figure 3d), except that during the later part of the simulation when M_{DHY} is decreasing, M_{DRGN} stays roughly constant. This difference in the later period of the simulation is due to the transfer of mass from M_{DHY} to M_{DRGN} as a result of the evaporation and/or sublimation of remnant anvils. M_{DRGN} is subject to dry deposition; however, this is a slow process, and hence, M_{DRGN} remains somewhat constant following the storm passage.

The amount of SAL_AR dust deposited to the ocean surface due to the dust removal processes (Figure 3c) is approximately 2 orders of magnitude greater than the amount of SAL_AR dust transported aloft by convective activity (Figure 3d). Calculating $M_{DRGN,LOFT}$ (equation (1)) reveals that TS Debby transported 0.04% of the total M_D amount present at the onset of the analysis period to the region above 7 km during the course of the simulation. Using NAMMA observations, *Twohy* [2015] reported 2 to 3 orders of magnitude less dust mass within anvil ice as compared to dust mass within the SAL. The results presented here are, therefore, in support of *Twohy* [2015], thus indicating that only a small fraction of SAL dust mass is transported to the upper troposphere by tropical storms. Despite this, the amount of dust lifted by Debby and other storms may still be important due to its ice-nucleating impact on upper level clouds [*Sassen et al.*, 2003] and the consequent influence on Earth's radiation budget [*Liou*, 1986; *Kim and Ramanathan*, 2008].

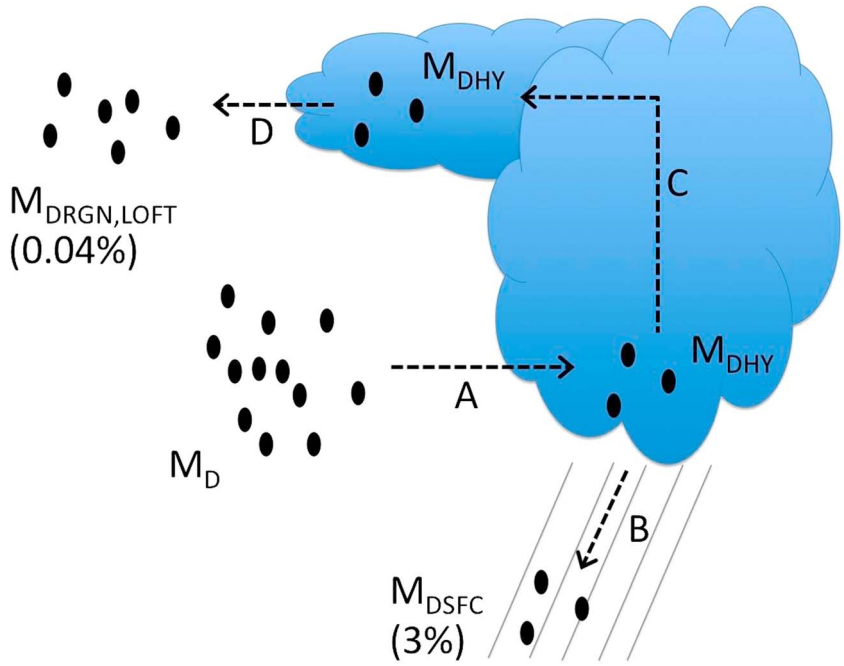

Figure 4. Schematic depicting microphysical processes that remove or transport dust. A represents entrainment into the storm, B represents wet and dry deposition, C represents convective transport, and D represents detrainment from the storm. Numbers in parentheses denote the portion of mass for the corresponding category compared to the initial amount of M_D introduced into the model at the onset of the analysis period (06 Z, 22 August).

5. Summary and Outlook

The RAMS CRM was utilized to investigate the impact of a TC on the vertical redistribution of dust. The simulations were configured using observed conditions during the period when TS Debby (2006) traversed through the SAL. Using unique dust tracking capabilities, dust budget analyses were performed to determine the relative amount of dust mass that is removed from the SAL and deposited on the ocean surface and the quantity of dust mass that is transported to upper levels of the troposphere.

When a TC passes through the SAL two pathways can redistribute dust. Dust resident in the atmosphere can be ingested by the storm due to horizontal convergence and transport through cloud base and cloud edges (Figure 4, "A"). A portion of the ingested dust may then be transferred to the surface by means of dust removal processes, wet and dry deposition (Figure 4, "B"), whereas another portion may be lofted to upper levels due to convective transport, sublimation, and evaporation (Figure 4, "C" and "D"). It was found that ~0.04% of the dust mass initially introduced into the SAL_AR at the start of the analysis period was transported to the upper troposphere, whereas ~3% was removed to the surface (Figure 4). Approximately 75 times more dust is therefore lost to the surface through wet and dry deposition than is lofted to the upper troposphere through convective activity. In spite of the small quantity of dust that is lofted, this amount may still be of importance due to its impacts on high altitude clouds and consequently the Earth's radiation budget and the climate.

Prior studies have estimated that the annual total dust mass removed from the SAL across the Atlantic Ocean is ~170 Tg [*Prospero*, 1996] and 139 Tg [*Yu et al.*, 2015]. The amount of dust redistributed by the TC in this study would be a small fraction of these amounts. Therefore, what is the role of TCs in the annual dust removal from the SAL? Other atmospheric phenomena such as congestus and deep tropical convection are also capable of vertically redistributing dust [*Mishra and Shibata*, 2012; *Sun et al.*, 2013]. As such, what are the relative impacts of more frequently occurring isolated and organized convection on dust redistribution and transport compared with that associated with the less frequent TC storms? Exploring trends relating the amounts of dust removed to the surface and dust transported aloft as a function of varying storm type, intensity, and size would provide valuable insight into the impact of all of these phenomena on ocean

fertilization and the Earth's radiation budget. Alternative satellite and field campaign data sets could be employed for model initialization to enhance the robustness of these kinds of comparisons. With increased computational capabilities we will be able to even further resolve cloud motions, perhaps without the need for nested grids.

Acknowledgments
This work was supported by the National Science Foundation awards AGS-1409686 and AGS-1408028. The authors thank Bruce Anderson of the National Aeronautics and Space Administration Langley Research Center for providing the Saharan dust data used in this study. Figure 1c in this study was produced with the Giovanni online data system, developed and maintained by the NASA GES DISC. Data required to recreate the results of this study are available upon request. Please contact the corresponding author at stephen.herbener@colostate.edu for assistance.

References

Albrecht, B. (1989), Aerosols, cloud microphysics, and fractional cloudiness, *Science*, *245*, 1227–1230.
Babin, S. M., J. A. Carton, T. D. Dickey, and J. D. Wiggert (2004), Satellite evidence of hurricane-induced phytoplankton blooms in an oceanic desert, *J. Geophys. Res.*, *109*, C03043, doi:10.1029/2003JC001938.
Chen, G., et al. (2011), Observations of Saharan dust microphysical and optical properties from the Eastern Atlantic during NAMMA airborne field campaign, *Atmos. Chem. Phys.*, *11*, 723–740, doi:10.5194/acp-11-723-2011.
Cotton, W. R., G. D. Alexander, R. Hertenstein, R. L. Walko, R. L. McAnelly, and M. Nicholls (1995), Cloud venting—A review and some new global annual estimates, *Earth Sci. Rev.*, *39*, 169–206, doi:10.1016/0012-8252(95)00007-0.
Cotton, W. R., et al. (2003), RAMS 2001: Current status and future directions, Meteorol, *Atmos. Phys.*, *82*, 5–29.
DeMott, P. J., M. P. Meyers, and W. R. Cotton (1994), Parameterization and impact of ice initiation processes relevant to numerical model simulations of cirrus clouds, *J. Atmos. Sci.*, *51*, 77–90.
DeMott, P. J., D. J. Cziczo, A. J. Prenni, D. M. Murphy, S. M. Kreidenweis, D. S. Thomson, R. Borys, and D. C. Rogers (2003), Measurements of the concentrations and composition of nuclei for cirrus formation, *Proc. Natl. Acad. Sci. U.S.A.*, *100*, 14,655–14,660, doi:10.1073/pnas.2532677100.
DeMott, P. J., et al. (2015), Integrating laboratory and field data to quantify the immersion freezing ice nucleation activity of mineral dust particles, *Atmos. Chem. Phys.*, *15*, 393–409, doi:10.5194/acp-15-393-2015.
Harrington, J. Y. (1997), The effects of radiative and microphysical processes on simulated warm and transition season Arctic stratus, PhD dissertation, Colorado State University, Atmospheric Science Paper 637, 289 pp.
Heymsfield, A. J., and G. M. McFarquhar (2001), Microphysics of INDOEX clean and polluted trade cumulus clouds, *J. Geophys. Res.*, *106*, 28,653–28,673, doi:10.1029/2000JD900776.
Hudson, J. G., and S. S. Yum (2002), Cloud condensation nuclei spectra and polluted and clean clouds over the Indian Ocean, *J. Geophys. Res.*, *107*, 8022, doi:10.1029/2001JD000829.
Kim, D., and V. Ramanathan (2008), Solar radiation budget and radiative forcing due to aerosols and clouds, *J. Geophys. Res.*, *113*, D02203, doi:10.1029/2007JD008434.
Liou, K.-N. (1986), Influence of cirrus clouds on weather and climate processes: A global perspective, *Mon. Weather Rev.*, *114*, 1167–1199, doi:10.1175/1520-0493(1986)114.
Maring, H., D. L. Savioe, M. A. Izaguirre, L. Custals, and J. S. Reid (2003), Vertical distributions of dust and sea-salt aerosols over Puerto Rico during PRIDE measured from a light aircraft, *J. Geophys. Res.*, *108*(D19), 8587, doi:10.1029/2002JD002544.
Mesinger, F., and A. Arakawa (1976), Numerical methods used in atmospheric models, GARP Publ. Ser. 17, WMO/ICSU Jt. Organ. Comm., 1, 1–65.
Meyers, M. P., R. L. Walko, J. Y. Harrington, and W. R. Cotton (1997), New RAMS cloud microphysics parameterization. Part II. The two-moment scheme, *Atmos. Res.*, *45*, 3–39.
Mishra, A. K., and T. Shibata (2012), Climatological aspects of seasonal variation of aerosol vertical distribution over central Indo-Gangetic belt (IGB) inferred by the space-borne lidar CALIOP, *Atmos. Environ.*, *46*, 365–375, doi:10.1016/j.amosenv.2011.09.052.
Molinari, J. (1985), A general form of Kuo's cumulus parameterization, *Mon. Weather Rev.*, *113*, 1411–1416.
Nguyen, L. T., J. Molinari, and D. Thomas (2014), Evaluation of tropical cyclone center identification methods in numerical models, *Mon. Weather Rev.*, *142*, 4326–4339, doi:10.1175/MWR-D-14-00044.1.
Prospero, J. M. (1996), Saharan dust transport over the North Atlantic Ocean and Mediterranean: An overview, in *The Impact of Desert Dust Across the Mediterranean*, edited by S. Guerzoni and R. Chester, pp. 133–151, Kluwer Acad., Netherlands.
Reale, O., K. M. Lau, A. da Silva, and T. Matsui (2014), Impact of assimilated and interactive aerosol on tropical cyclogenesis, *Geophys. Res. Lett.*, *41*, 3282–3288, doi:10.1002/2014GL059918.
Reddy, K., D. V. Phani Kumar, Y. Nazeer Ahammed, and M. Naja (2013), Aerosol vertical profiles strongly affect their radiative fuction uncertainties: study by using ground-based lidar and other measurements, *Remote Sens. Lett.*, *4*(10), 1018–1027, doi:10.1080/2150704X.2013.828182.
Saleeby, S. M., and W. R. Cotton (2004), A large-droplet mode and prognostic number concentration of cloud droplets in the Colorado State University Regional Atmospheric Modeling System (RAMS). Part I: Module Descriptions and Supercell Test Simulations, *J. Appl. Meteorol.*, *43*, 182–195.
Saleeby, S. M., and S. C. van den Heever (2013), Developments in the CSU-RAMS aerosol model: Emissions, nucleation, regeneration, deposition, and radiation, *J. Appl. Meteorol. Climatol.*, *52*, 2601–2622.
Sassen, K., P. J. DeMott, J. M. Prospero, and M. R. Poellot (2003), Saharan dust storms and indirect aerosol effects on clouds: CRYSTAL-FACE results, *Geophys. Res. Lett.*, *30*(12), 1633, doi:10.1029/2003GL017371.
Seigel, R. B., and S. C. van den Heever (2012), Dust lofting and ingestion by supercell storms, *J. Atmos. Sci.*, *69*, 1453–1473, doi:10.1175/JAS-D-11-0222.1.
Seigel, R. B., S. C. van den Heever, and S. M. Saleeby (2013), Mineral dust indirect effects and cloud radiative feedbacks of a simulated idealized nocturnal squall line, *Atmos. Chem. Phys.*, *13*, 4467–4485.
Stokowski, D. (2005), The addition of the direct radiative effect of atmospheric aerosols into the Regional Atmospheric Modeling System (RAMS), MS thesis, Dep. of Atmospheric Science, Colorado State University, Atmospheric Science Paper 637, 89 pp.
Sun, X. Y., Y. Yin, Y. Sun, Y. Sun, W. Liu, and Y. Han (2013), Seasonal and vertical variations in aerosol distribution over Shijiazhuang, China, *Atmos. Environ.*, *81*, 245–252, doi:10.1016/j.atmosenv.2013.08.009.
Twohy, C. H. (2015), Measurements of Saharan dust in convective clouds over the tropical eastern Atlantic Ocean, *J. Atmos. Sci.*, *72*, 75–81, doi:10.1175/JAS-D-14-0133.1.
Twohy, C. H., et al. (2009), Saharan dust particles nucleate droplets in eastern Atlantic clouds, *Geophys. Res. Lett.*, *36*, L01807, doi:10.1029/2008GL035846.
Twomey, S. (1974), Pollution and the planetary albedo, *Atmos. Environ.*, *8*, 1251–1256.

Walko, R. L., W. R. Cotton, M. P. Meyers, and J. Y. Harrington (1995), New RAMS cloud microphysics parameterization. Part I. The single-moment scheme, *Atmos. Res.*, *38*, 29–62.

Yu, H., et al. (2015), Quantification of trans-Atlantic dust transport from seven-year (2007–2013) record of CALIPSO lidar measurements, *Remote Sens. Environ.*, *159*, 232–249, doi:10.1016/j.rse.2014.12.010.

Zarzycki, C., and T. C. Bond (2010), How much can the vertical distribution of black carbon affect its global radiative forcing? *Geophys. Res. Lett.*, *37*, L20807, doi:10.1029/2010GL044555.

Zipser, E. J., et al. (2009), The Saharan air layer and the fate of African easterly waves, *Bull. Am. Meteorol. Soc.*, *90*, 1137–1156, doi:10.1175/2009BAMS2728.1.